

## Acoustic emission monitoring of composite marine propeller blades using embedded piezoelectric sensors and hydrophones

Huijer, A.J.; Kassapoglou, C.; Pahlavan, Lotfollah

**DOI**

[10.58286/29607](https://doi.org/10.58286/29607)

**Publication date**

2024

**Document Version**

Final published version

**Published in**

e-Journal of Nondestructive Testing

**Citation (APA)**

Huijer, A. J., Kassapoglou, C., & Pahlavan, L. (2024). Acoustic emission monitoring of composite marine propeller blades using embedded piezoelectric sensors and hydrophones. *e-Journal of Nondestructive Testing*, 1-8. <https://doi.org/10.58286/29607>

**Important note**

To cite this publication, please use the final published version (if applicable). Please check the document version above.

**Copyright**

Other than for strictly personal use, it is not permitted to download, forward or distribute the text or part of it, without the consent of the author(s) and/or copyright holder(s), unless the work is under an open content license such as Creative Commons.

**Takedown policy**

Please contact us and provide details if you believe this document breaches copyrights. We will remove access to the work immediately and investigate your claim.

# Acoustic emission monitoring of composite marine propeller blades using embedded piezoelectric sensors and hydrophones

Arnaud HUIJER<sup>1\*</sup>, Christos KASSAPOGLOU<sup>2</sup>, Lotfollah PAHLAVAN<sup>1</sup>

<sup>1</sup> Delft University of Technology, Faculty of Mechanical Engineering, Delft, the Netherlands

<sup>2</sup> Delft University of Technology, Faculty of Aerospace Engineering, Delft, the Netherlands

\*Corresponding author: a.j.huijer@tudelft.nl

**Abstract.** The current research investigates the measurement of acoustic emissions (AE) signals in composite marine propeller blades using embedded piezoelectric transducers. A full-scale glass-fibre polymer composite propeller blade is suspended in a tank filled with artificial seawater. The propeller blade contains 24 embedded piezoelectric sensors that were installed between laminas during manufacturing. Additionally, the tank includes an array of hydrophones for comparison of the results. AE signals are simulated on the blade by the actuation of one of the embedded transducers in a manner that is representative of damage in the blade. The measured AE signals are assessed for their amplitude and frequency content. The results demonstrate the feasibility of measuring AE signals in composite marine propeller blades using both the embedded and external measurement systems.

**Keywords:** acoustic emission, composite marine propeller, embedded sensor, damage detection, piezoelectric sensor

## 1. Introduction

The reduction of greenhouse gas emissions and environmental noise is important in the marine industry [1,2]. In this context, marine propellers can be improved to reduce both carbon emissions as well as environmental noise. These improvements can be attained by manufacturing marine propellers out of fibre-reinforced composites instead of metals. Composite materials allow for a propeller blade that can alter its shape when being loaded. This means that the blade can become more efficient in off-design conditions, reducing carbon emissions of the propulsion system. Furthermore, the flexible blade can reduce pressure pulses at the tip of the blade, reducing underwater radiated noise [3]. Additional advantages of using composite materials for marine propeller blades are a reduction of



weight, a smaller electrical signature and the possibility for the embedding of sensors [4]. Because of these advantages, there are ongoing developments in the manufacture and use of composite marine propeller blades. One of the hurdles to successful implementation is the lack of in-situ knowledge on the degradation and fatigue of composite marine propeller blades.

To overcome this hurdle, a structural health monitoring (SHM) approach is considered for the blade. Methods can be by measuring strains and vibrations through digital image correlation [5], strain gauges [6,7], optical fibres [6,8–11] or piezoelectric sensors [12,13]. Another option could be material characterisation through ultrasonic guided waves [14]. Alternatively, a very direct indication of the creation of damage can be obtained through the measurement of acoustic emissions.

Acoustic emissions (AE) are elastic bursts originating from the initiation and progression of damage. In the case of composite materials, AE are typically propagating as ultrasonic guided waves, with different damage mechanisms having specific signatures in terms of frequency content and amplitude, among others [15]. In large-scale composite marine structures, AE has been monitored in partial hull structures [16], while results regarding tidal turbines are expected [17]. Regarding composite marine propeller blades, the authors performed a prior study [18] indicating the feasibility of measuring AE using embedded piezoelectric sensors. The first results on a full-scale composite marine propeller blade with embedded piezoelectric sensors are presently underway.

In this research, acoustic emissions, emitted through active pulsing, have been measured on a composite marine propeller blade using embedded piezoelectric sensors and remote hydrophones. The use of these two measurement systems allows for the comparison of measurement sensitivity of AE.

The paper is organised as follows: in Section 2, the methodology is explained for the measurement of AE using embedded piezoelectric sensors and using hydrophones. Further, the experimental procedure is clarified. Section 3 highlights the results, showing the measured waveforms and signal amplitude changes over measurement distance and sensor type. In Section 4, conclusions are given, followed by recommendations for future research.

## 2. Methodology

In this research, acoustic emissions are recorded by two different means; embedded piezoelectric sensors and external hydrophones. Both measurement types are subject to different forms of transfer functions and wave propagation effects.

For the embedded piezoelectric sensors, the measured signal can be described as follows (Equation 1):

$$P_p(\mathbf{x}_R, \mathbf{x}_S, \omega) = \sum_{i=1}^n D_i(\mathbf{x}_R, \omega) W_i(\mathbf{x}_R, \mathbf{x}_S, \omega) \zeta_i(\mathbf{x}_S) S(\mathbf{x}_S, \omega) + P_N(\mathbf{x}_R, \omega). \quad (1)$$

In this equation, the measurement signal is denoted by  $P_p$  as function of source location  $\mathbf{x}_S$ , measurement location  $\mathbf{x}_R$  and circular frequency  $\omega$ . For embedded piezoelectric sensors, the acoustic emission source  $S(\mathbf{x}_S, \omega)$  propagates throughout the blade as an elastic guided wave. There can be multiple guided wave modes constituting the measurement. This is indicated by the summation over modes  $i = 1..n$ . Note that sensor transfer function  $D_i(\mathbf{x}_R, \omega)$ , wave propagation transfer function  $W_i(\mathbf{x}_R, \mathbf{x}_S, \omega)$  and components of the source

$\zeta_i(\mathbf{x}_S)$  are dependent on the wave mode. Additionally, embedded piezoelectric sensors can be sensitive to noise, such as electromagnetic interference, acoustic reflections and external ultrasound sources.

For hydrophone measurement  $P_h$ , a different equation is set up (Equation 2):

$$P_h(\mathbf{x}_R, \mathbf{x}_S, \omega) = D_h(\mathbf{x}_R, \omega)W_h(\mathbf{x}_R, \mathbf{x}_S, \omega)\zeta_h(\mathbf{x}_S, \omega)\mathcal{S}(\mathbf{x}_S, \omega) + P_N(\mathbf{x}_R, \omega). \quad (2)$$

Here, the wave propagation from source to sensor is through an acoustic pressure wave medium with transfer function  $W_h(\mathbf{x}_R, \mathbf{x}_S, \omega)$  and with hydrophone transfer function  $D_h(\mathbf{x}_R, \omega)$  and a source sensitivity to acoustic waves  $\zeta_h(\mathbf{x}_S, \omega)$ .

In the current work, acoustic emissions are simulated through using one of the sensors as an actuator for sending out a signal. This means that the source function itself contains a transfer function  $D_m^{-1}(\mathbf{x}_S, \omega)$  from the electrical input signal  $\mathcal{S}(\mathbf{x}_S, \omega)$  to the mechanical excitation in mode  $m$ . This is described in Equation 3:

$$\zeta_m(\mathbf{x}_S, \omega)\mathcal{S}(\mathbf{x}_S, \omega) = D_m^{-1}(\mathbf{x}_S, \omega)\mathcal{S}(\mathbf{x}_S, \omega). \quad (3)$$

### 2.1. Experimental set-up

The experimental set-up was as follows: a glass-fibre composite marine propeller blade [3] with 24 embedded piezoelectric sensors (PIC255 material, diameter 5mm, thickness 0.25mm) was lowered into a salt water tank (53mS/cm at 25°C). The tank also contained an array of 8 hydrophones of type VS150-WIC. An illustration of the setup can be seen in Figure 1. Detailed photographs can be seen in Figure 2.

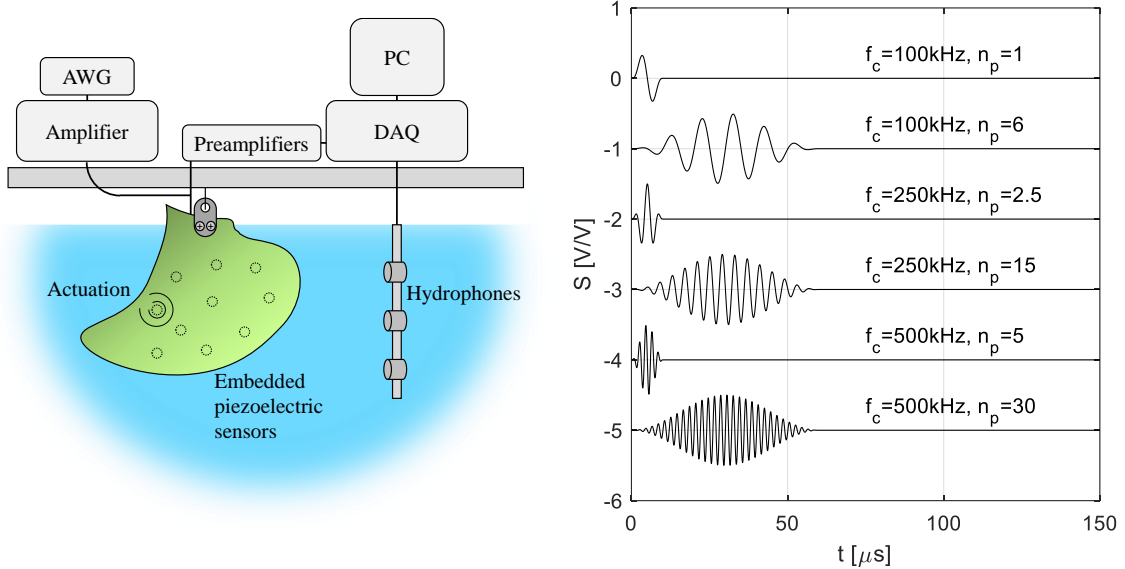


**Fig. 1.** The left figure shows a graphical illustration on exciting and measuring acoustic emissions through embedded piezoelectric sensors and hydrophones. Note that the abbreviations AWG, DAQ and PC stand for arbitrary waveform generator, data acquisition system and personal computer respectively. The right figure describes the signals sent out by the waveform generator. The accompanying text mentions the centre frequency ( $f_c$ ) and number of periods ( $n_p$ ) in the signal.

For actuation, signals of 100-250-500kHz were chosen in a wide and narrow-band form. These are visualised in Figure 1. It was considered that these ranges of frequency can depict acoustic emissions from matrix cracking, delamination and fibre-breaking respectively. Actuation was performed using a Siglent SDG10251 arbitrary waveform generator, with a 1V peak-to-peak amplitude, amplified 34dB by a Falco WMA-300 power amplifier. The measurements from the embedded piezoelectric sensors were amplified 40dB using Vallen AEPH5H preamplifiers. The data acquisition system for both embedded piezoelectric

sensors and hydrophones was a Vallen AMSY-6. These systems are denoted 1-5 in Figure 2.

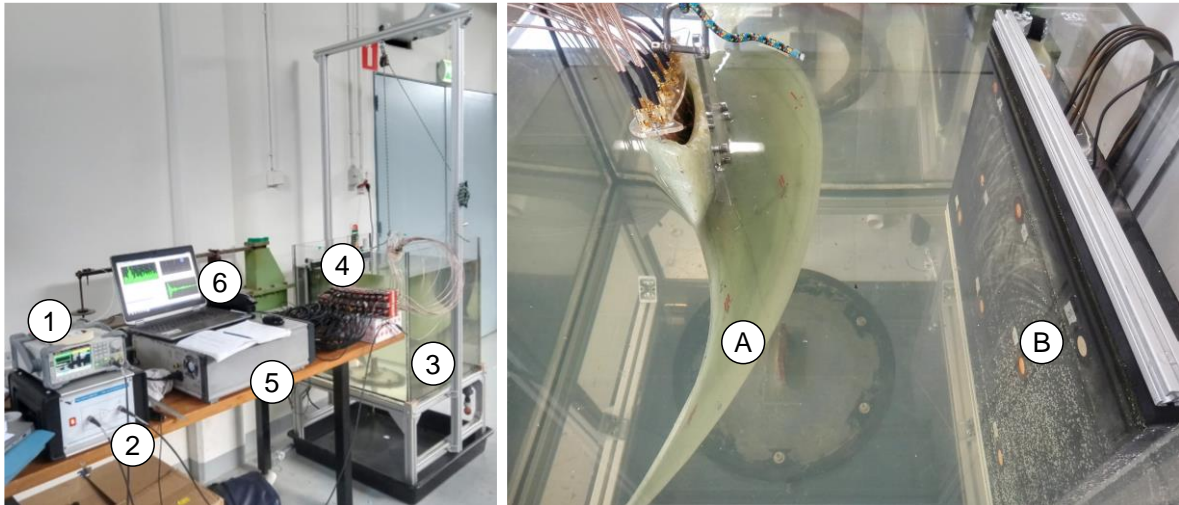


**Fig. 1.** Measurement set-up. On the left photograph is visible from 1 to 6: the waveform generator, the voltage amplifier, the water tank with propeller blade and hydrophones, the preamplifiers for the sensors, the data acquisition system and the measurement computer. The right photograph highlights the propeller blade (A) and the hydrophone array (B).

The data acquisition was hit-based and had the following parameters: The sample rate was 2Mhz, with a total duration of 2048 $\mu$ s. A digital frequency band-pass filter was applied, ranging from 25kHz to 850kHz. The static threshold was set at 40dB(ref 1 $\mu$ V) while the dynamic threshold, or threshold to noise ratio, was set at 6dB. Rearm time and duration discretisation time were both 250 $\mu$ s. Pretrigger duration was 150 $\mu$ s.

### 3. Results

The signals that are recorded are assessed in the following way: Firstly, for the embedded piezoelectric sensors, the signals are split in time to distinguish between components. For the hydrophones, no such separation is necessary. Secondly, the maximum of amplitudes are assessed for the elastic guided wave measurement of the embedded sensors and the acoustic wave measurement of the hydrophones. Spatial variation is shown by contour plots. Thirdly, trends have been analysed from these amplitudes, using actuation signals with different centre frequencies and bandwidth.

For an excitation at sensor 10, a visualisation of the normalised signal amplitude over time is shown in Figure 3:

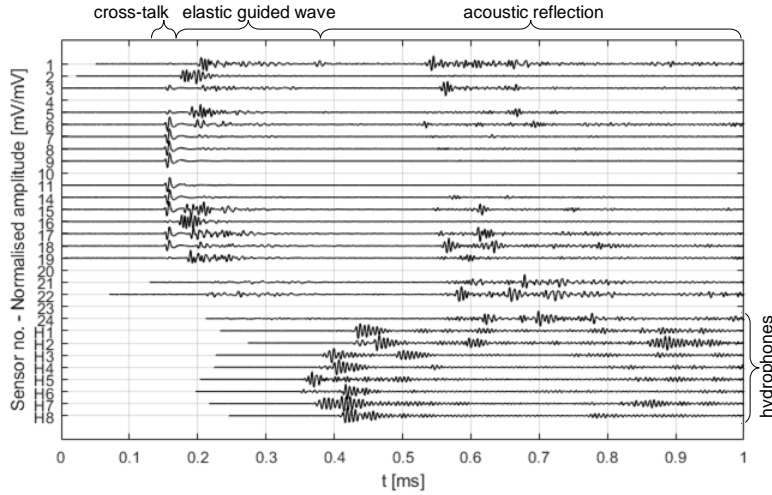


**Fig. 2.** Normalised signals over time, measured by embedded piezoelectric sensors and hydrophones. In this case, actuation was at sensor 3, using a 2.5-period 250kHz signal. Upper accoladed regions denote the intervals in time that are related to different manifestations of measurement of the actuation signal.

In this figure, embedded piezoelectric sensors 1-24 are included together with hydrophones H1-H8. The time axis starts when the earliest sensor starts recording. For the embedded sensors, the signal contains multiple components. These are the pretrigger interval, cross-talk, elastic guided wave interval, and acoustic reflection interval. The cross-talk can be seen by the non-dispersed part of the signal around  $t = 150\mu\text{s}$  that is being recorded by multiple sensors without time delay. In the measurement of the elastic guided wave, the signals show dispersive behaviour and time delays that increase with increasing distance between actuation and sensor. Note that both cross-talk and elastic guided waves are not recorded by all embedded sensors. The acoustic reflections from the water tank arrive later and appear to be of fairly large amplitude, recording at sensors that did not capture the elastic guided wave. The hydrophones measure signals at a delay in time which is roughly half-way in between the measurement of cross-talk and acoustic reflection of the embedded sensors. The spread in measuring hydrophone signals can be attributed to multiple propagation paths that an acoustic wave can have in a confined tank.

To assess the amplitudes, the signals measured by the embedded piezoelectric sensors are separated, as shown in Table 1.

**Table 1:** Intervals in the measurements of embedded piezoelectric sensors attributed to pretrigger, cross-talk, elastic guided waves and acoustic reflection.

Interval [ $\mu\text{s}$ ]	Pretrigger	Cross-talk	Elastic guided wave	Acoustic reflection
<b>Wide-band</b>	0-145	145-180	180-350	350-end
<b>Narrow-band</b>	0-120	120-210	210-350	350-end

The length of the cross-talk interval is comparable to the duration of the input excitation (Figure 1). Further, for the case of narrow-band excitation, the elastic guided wave is partly overlapping with the cross-talk. Hence for the elastic guided wave interval, the starting time is additionally delayed. This can influence the assessment of amplitude of the elastic guided waves for narrow-band input signals.

For the assessment of amplitudes throughout the blade, contour plots have been made. An example can be seen in Figure 4:

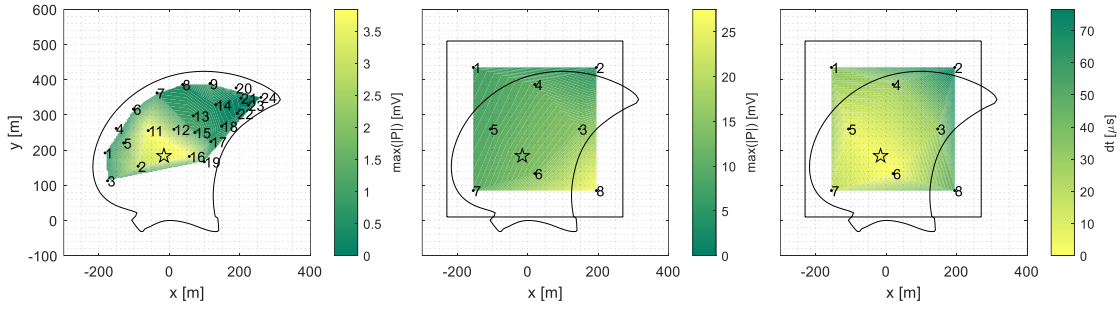


**Fig. 3.** Contour plots of measurements by embedded piezoelectric sensors and hydrophones. In this case, actuation was at sensor 10, using a 2.5-period 250kHz signal. The actuation location is described by the  $\star$ . Sensor locations are denoted by a  $\bullet$  and the sensor number. The left figure shows the maximum amplitude measured by the embedded piezoelectric sensors in the interval 180-350 $\mu$ s. The middle figure shows the maximum amplitude measured by the hydrophones. The right figure shows the time delay from first arrival of the hydrophones.

In this figure it can be seen that when measuring with embedded piezoelectric sensors, the sensors in the immediate vicinity of the actuation are well capturing the acoustic emission. For increasing distance, amplitude  $\max(|P|)$  decreases. For the hydrophones this behaviour is not encountered, with the amplitudes appearing seemingly unrelated to the actuation location. However, there is consistency when considering the time delay  $dt$  with respect to the first hydrophone recording the signal. Here an increase in time delay relates to an increase in distance from the actuation point.

To investigate the behaviour of the sensors (and actuation) over a range of frequencies, three embedded piezoelectric sensors and hydrophones close by the actuator were assessed. This can be seen in Figure 5.

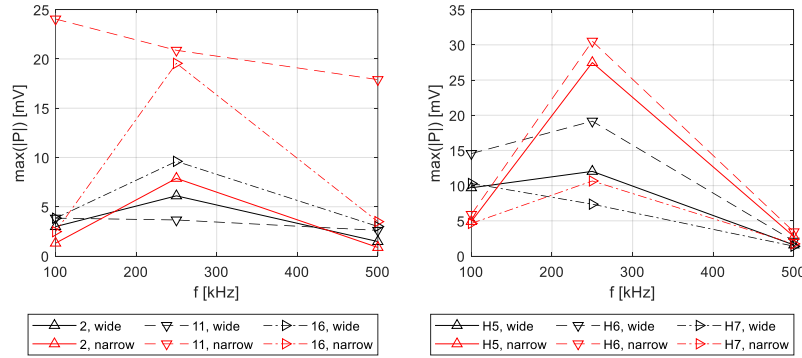


**Fig. 4.** Maximum amplitudes for sensors close to the actuation location, given varying actuation frequency and bandwidth. The left graph shows the amplitude for elastic guided waves measured by embedded piezoelectric sensors. The right graph displays the amplitudes from the hydrophones.

The results shows that in general, the measurements for 250kHz are with higher amplitude than those of 100kHz and 500kHz. This can be due to higher sensitivity of the actuator at that frequency. Stronger sensitivity of the sensors for this frequency is not directly anticipated. This is because similar behaviour takes place at both the embedded piezoelectric sensors and the hydrophones, and it is known that the hydrophones are not particularly sensitive at this frequency. What further strikes out is the comparatively higher sensitivity of narrow-band signals at this frequency. It is considered that a narrow-band signal suffers less from dispersion effects but this should only manifest itself with the embedded piezoelectric sensors.

#### 4. Conclusions and further research

In this research, simulated acoustic emissions from a composite marine propeller blade were assessed using embedded piezoelectric sensors and hydrophones. The acoustic emissions were simulated using one of the piezoelectric transducers as an actuator. It was found that the measurement of elastic guided waves using the embedded piezoelectric sensors was contaminated by electrical cross-talk from the actuator and by reflections of the acoustic wave from the tank walls. When windowing out these sources of noise, the drop in amplitude over the blade correlated with an increase of distance from the source to sensor. For the hydrophones, it was noted that there was no cross-talk being measured. Further, the amplitude of the measurement with the hydrophones was not consistent considering its projected location with respect to the source at the blade. However, the recorded time delay did show a consistency, with the time delay increasing with an increasing distance from source to hydrophone.

The investigation highlights initial results and particularities from measuring acoustic emissions with both embedded piezoelectric sensors and remote hydrophones. It is envisioned that the results can further be used to assess localisation of acoustic emissions using these types of sensors.

#### Acknowledgements

This research has been performed in the context of ECoProp project sponsored by the Dutch Research Council (NWO) and a consortium of industrial partners. Additionally Wouter de Bles is acknowledged for his contribution to the fabrication of the test blade with embedded sensors. Furthermore Filippo Riccioli is acknowledged for his contributions regarding the hydrophones used.

#### References

- [1] IMO 2023 Revised Guidelines for the Reduction of URN from Shipping to Address Adverse Impacts on Marine Life *Int. Marit. Organ. MEPC.1/Cir* 1–19
- [2] IMO 2023 IMO Strategy on Reduction of GHG Emissions from Ships, Resolution **MEPC.377(80) 4** 88–100
- [3] Maljaars P J and Dekker J A 2015 Hydro-elastic analysis of flexible marine propellers *Maritime Technology and Engineering - Proceedings of MARTECH 2014: 2nd International Conference on Maritime Technology and Engineering* pp 705–16
- [4] Young Y L, Motley M R, Barber R, Chae E J and Garg N 2016 Adaptive composite marine propulsors and turbines: Progress and challenges *Appl. Mech. Rev.* **68**
- [5] Maljaars P, Bronswijk L, Windt J, Grasso N and Kaminski M 2018 Experimental validation of fluid-structure interaction computations of flexible composite propellers in open water conditions using BEM-FEM and RANS-FEM methods *J. Mar. Sci. Eng.* **6**
- [6] Zetterlind V E, Watkins S E and Spoltman M W 2003 Fatigue testing of a composite propeller blade using fiber-optic strain sensors *IEEE Sens. J.* **3** 393–9
- [7] Tian J, Croaker P, Zhang Z and Hua H 2016 Dynamic strain measurements of marine propellers under non-uniform inflow *Journal of Physics: Conference Series* vol 744 (Institute of Physics Publishing) p 012094
- [8] Seaver M, Trickey S T and Nichols J M 2006 Strain measurements from FBGs embedded in rotating composite propeller blades *Optics InfoBase Conference Papers*

- (Optical Society of America (OSA)) p ThD2
- [9] Javdani S, Fabian M, Carlton J S, Sun T and Grattan K T V 2016 Underwater Free-Vibration Analysis of Full-Scale Marine Propeller Using a Fiber Bragg Grating-Based Sensor System *IEEE Sens. J.* **16** 946–53
  - [10] Ding G, Yan X, Gao X, Zhang Y and Jiang S 2022 Reconstruction of propeller deformation based on FBG sensor network *Ocean Eng.* **249**
  - [11] Shamsuddoha M, Prusty G B, Maung P T, Phillips A W and St John N A 2022 Smart monitoring of a full-scale composite hydrofoil manufactured using automated fibre placement under high cycle fatigue *Smart Mater. Struct.* **31**
  - [12] Hamada R, Ogura T, Fujita S, Murayama H, Yamatogi T, Inoue T, Hayashi K, Takahara M, Goto K and Furukawa K 2023 Structural Health Monitoring of CFRP Propellers by Piezoelectric Line Sensors *Structural Health Monitoring* ed S Farhangdoust, A Guemes and F-K Chang (Stanford: DEStech Publications, Inc. 439 North Duke Street Lancaster, Pennsylvania 17602 U.S.A.) pp 408–16
  - [13] de Bles W 2022 Dynamic response reconstruction of an FRC blade with embedded piezoelectric sensors *MSc Thesis*
  - [14] Adams M G A, Huijjer A J, Kassapoglou C, Vaders J A A and Pahlavan L 2024 In-Situ Non-Destructive Stiffness Assessment of Fiber Reinforced Composite Plates Using Ultrasonic Guided Waves *Sensors (Switzerland)* 1–19
  - [15] Saeedifar M and Zarouchas D 2020 Damage characterization of laminated composites using acoustic emission: A review *Compos. Part B Eng.* **195** 108039
  - [16] Raju, Azmi A I and Prusty B G 2012 Acoustic emission techniques for failure characterisation in composite top-hat stiffeners *J. Reinf. Plast. Compos.* **31** 495–516
  - [17] Davies P, Dumergue N, Arhant M, Nicolas E, Paboeuf S and Mayorga P 2022 Material and structural testing to improve composite tidal turbine blade reliability *Int. Mar. Energy J.* **5** 57–65
  - [18] Huijjer A, Zhang X, Kassapoglou C and Pahlavan L 2022 Feasibility evaluation for development of composite propellers with embedded piezoelectric sensors *Mar. Struct.* **84** 103231